JVSTB Journal of Vacuum Science & Technology B

Submillimeter-wavelength plasma chemical diagnostics for semiconductor manufacturing

Eric C. Benck, Guerman Yu. Golubiatnikov, Gerald T. Fraser, Bing Ji, Stephen A. Motika, and Eugene J. Karwacki

Citation: Journal of Vacuum Science & Technology B **21**, 2067 (2003); doi: 10.1116/1.1605431
View online: http://dx.doi.org/10.1116/1.1605431
View Table of Contents: http://scitation.aip.org/content/avs/journal/jvstb/21/5?ver=pdfcov
Published by the AVS: Science & Technology of Materials, Interfaces, and Processing

Submillimeter-wavelength plasma chemical diagnostics for semiconductor manufacturing

Eric C. Benck[a)]
Physics Laboratory, Atomic Physics Division, Mail Stop 8421, National Institute of Standards and Technology, Gaithersburg, Maryland 20899

Guerman Yu. Golubiatnikov[b)]
Physics Laboratory, Optical Technology Division, Mail Stop 8441, National Institute of Standards and Technology, Gaithersburg, Maryland 20899

Gerald T. Fraser[c)]
Physics Laboratory, Optical Technology Division, Mail Stop 8441, National Institute of Standards and Technology, Gaithersburg, Maryland 20899

Bing Ji, Stephen A. Motika, and Eugene J. Karwacki
Air Products and Chemicals, Inc., 7201 Hamilton Boulevard, Allentown, Pennsylvania 18195

(Received 24 January 2003; accepted 7 July 2003; published 15 September 2003)

Submillimeter-wavelength linear-absorption spectroscopy has been applied to the chemical diagnostics of reactive-ion etching plasmas in a modified capacitively coupled gaseous electronics conference reactor. Approximately 1 mW of narrow-band (<10 kHz) submillimeter radiation between 450 and 750 GHz is produced using a backward-wave oscillator (BWO). The BWO is frequency stabilized to a harmonic of a 78–118 GHz frequency synthesizer. The submillimeter method offers high sensitivity for the ≈ 1 MHz linewidth, Doppler-broadened absorption lines typical of gas-phase molecules at a total pressure of less than 133 Pa (1 Torr). A large number of molecules can be detected, limited primarily by the need for a permanent electric dipole moment and for accurate line frequency predictions, the latter of which are often available in the literature. The capabilities of the diagnostic method have been demonstrated by the following three applications: (1) the measurement of water-vapor contamination in the reactor and in the precursor gas by monitoring a rotational transition of H_2O in the reactor just prior to the initiation of the plasma; (2) the assessment of progress in the cleaning of the reactor by an O_2/Ar plasma after a fluorocarbon plasma etch by monitoring the build up of the concentration of O_3 and the depletion of the concentration of CF_2O in the plasma; and (3) the determination of the endpoint in the etching of a SiO_2 thin film on silicon by an octafluorocyclobutane/O_2/Ar plasma by monitoring the decrease in the concentration of SiO in the plasma. The last observation is made possible by the large electric dipole moment for SiO of 1×10^{-29} C m (3.1 D), which gives a low minimum detectable number density for the radical of 2×10^{7} cm^{-3} for an optical pathlength of 39 cm. © *2003 American Vacuum Society.* [DOI: 10.1116/1.1605431]

I. INTRODUCTION

Progress in plasma processing for semiconductor manufacturing[1] is becoming increasingly dependent on *in situ* diagnostics, i.e., on the ability to quantitatively and nonintrusively measure physical and chemical properties of the plasma, such as temperature, concentration, and spatial distribution of electrons and molecules.[1–3] The information obtained from such measurements aids the advancement and validation of complex computational plasma models. These models[4,5] are required to respond to industry demands for better plasma processing technology for semiconductor manufacturing. The technology needs include: (1) ensuring good etch uniformity over increasingly larger wafer surface areas, (2) being able to produce smaller, more complex, and large aspect-ratio features, (3) reducing chamber cleaning time and frequency, (4) decreasing the consumption of expensive process gases, and (5) eliminating toxic, atmospheric greenhouse contributing, or stratospheric-ozone-depleting effluent emissions.

A number of techniques have been developed for semiconductor plasma diagnostics, differing in their generality, sensitivity, and specificity. Many of these techniques have emphasized the measurement of the chemical composition of the plasma. Such chemical diagnostic techniques include mass spectrometry, various linear absorption spectroscopies, laser-induced fluorescence, optical-emission spectroscopy, cavity ring-down spectroscopy,[6] and negative-ion photodetachment methods.[7] Linear-absorption spectroscopy is particularly important, as it provides absolute chemical quantification, albeit, of the average number density along the optical path. In principle, spatial chemical information is also available by making a set of measurements along distinct

[a)]Electronic mail: eric.benck@nist.gov
[b)]Present address: Institute of Applied Physics, Russian Academy of Sciences, Uljanov Street 46, 603600 Nizhnii Novgorod, Russia; electronic mail: guerman@nist.gov
[c)]Electronic mail: gerald.fraser@nist.gov

optical paths. Tomographic methods, such as the Abel transform, could be used to invert the results of measurements into spatial information. However, this approach has yet to be implemented in the laboratory.

Plasma-diagnostic measurements based on linear absorption spectroscopy have received significant attention in the infrared and optical spectral regions due to the availability of the necessary instrumentation. Midinfrared diode-laser spectroscopy has been used to successfully investigate fluorocarbon and hydrofluorocarbon-based etching plasmas.[8–11] However, the measurements are impeded by the need to positively identify a specific rotationally resolved absorption line from among the plethora of nearby lines. The spectral line density is typically high due to the presence of a common C–F stretch chromophore present in the precursor and many of the decomposition and polymerization products. For instance, Schaepkens *et al.*[12] found that the presence of CF_2O absorptions limited their ability to monitor CF and CF_2 using infrared laser absorption spectroscopy. Moreover, poor wavelength metrology in the infrared spectral region compounds the problem by making it difficult to transfer measurements between laboratories. Additional complications come from the poor frequency coverage, limited scanning capabilities, and multimode behavior of midinfrared, lead–salt diode lasers, which are typically used in the measurements. In addition, there also is a lack of accurate values for the absolute line strengths of free radicals and ions.

Visible and ultraviolet absorption spectroscopy using laser or broadband light sources have also been extensively applied toward understanding the chemical composition of semiconductor plasmas. Similar to infrared laser absorption spectroscopy, the necessary fundamental spectroscopic data are often lacking, particularly accurate values for absorption cross sections. Such data are required to obtain reliable concentration information. Additionally, the electronic absorption features probed in the visible and ultraviolet are often diffuse or blended with diffuse background features, making it difficult to determine a value for the integrated band strength, which is proportional to the average number density along the optical path. Also, a number of important plasma species do not have the intense visible or ultraviolet absorption spectra necessary for quantitative measurements.

Long-wavelength microwave to far-infrared (millimeter or submillimeter wave) absorption techniques have been virtually unexplored for semiconductor-processing plasma diagnostics. The lack of interest may be due in part to the poor spatial resolution at these wavelengths. For example, spatial resolution is limited by diffraction to approximately 1 cm at 1 THz for a 30 cm pathlength through a plasma reactor. However, for many applications spatial information is of less interest compared to chemical speciation and quantification. Also, submillimeter methods can be used even with small electrode gaps, as found in some reactors. The low-frequency cutoff for an infinite parallel-plate waveguide is less than 150 GHz for the TE_0 mode of a 2 mm gap and negligible for the dominant TM_0 mode. This ensures efficient transmission, assuming initial orientation of the electric field of the submillimeter radiation approximately normal to the electrode planes. Of course, the transmission properties of this parallel-plate waveguide will be complicated by the presence of the Si wafer and its coatings and the dielectric materials associated with the electrostatic chuck.

Unfamiliarity with the submillimeter and millimeter wavelength technology may have limited its acceptance, as the only published work in this area for plasma diagnostics appears to be the measurements of Chew *et al.*[13] in which SiO was detected and monitored using a rotational transition $(J=2-1)$ near 87 GHz in an electron cyclotron resonance plasma, under conditions appropriate for investigating plasma-enhanced chemical vapor deposition (CVD) of silicon oxide films. The measurements yielded average absolute number densities of SiO along the optical path for total pressures of the order of 1 Pa. Sensitivities as low as 1×10^{11} cm^{-2} for the product of the pathlength times the number density were achieved.

In the present work, the submillimeter wavelength linear absorption spectroscopy technique, which is based on backward-wave oscillators (BWOs), is applied to the chemical diagnostics of semiconductor etching plasmas. The BWOs used in the present study are spectrally narrow ($<$10 kHz) coherent radiation sources producing continuous-wave radiation from 60 to 850 GHz. The submillimeter technique has significant advantages over infrared, visible, and ultraviolet absorption methods for plasma diagnostics. These include excellent frequency metrology, referenced to atomic clocks, high spectral resolution for line shape studies, and the availability of accurate cross-section data from laboratory Stark-effect measurements. The excellent frequency metrology guarantees the identity of the molecular absorption peaks. Line shape studies allow the determination of the Doppler linewidths of the lines, which can potentially furnish a direct measure of the translational temperature of the plasma. Stark-effect measurements, from fundamental microwave spectroscopy studies, provide the molecular electric dipole moment and thus the rotational transition moment, without knowledge of the concentration, allowing the accurate calculation of the cross section of a rotational transition even for unstable free radicals.

The BWO-based technique is easy to implement, particularly below 180 GHz where the radiation sources and frequency stabilization electronics are encapsulated in a commercial package. One drawback of the technique is the difficulty in determining an absolute column density and thus the mean reactor number density of the species monitored. The measurement of the absolute column density requires determining an accurate value for the fractional absorption of the submillimeter beam by a molecular line, and is not fully addressed in the present article, but will be the topic of a future publication.

Essentially all diatomic and polyatomic molecules with an electric dipole moment have an absorption line accessible between 100 and 850 GHz, with the notable exception of HF, OH, and other diatomic hydrides, which have moments of inertia too small for submillimeter absorption. Some nonpo-

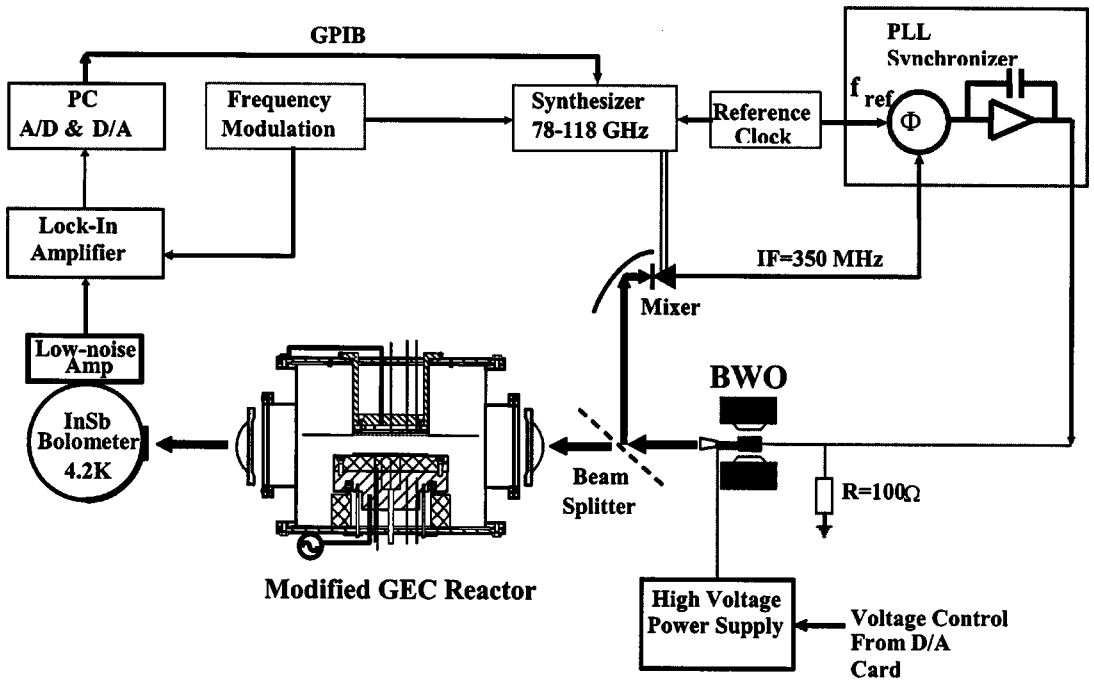

FIG. 1. Schematic diagram of the submillimeter spectrometer and the GEC reactive ion etch reactor.

lar molecules and atoms also have spectral absorptions in this region, including molecular oxygen, atomic carbon, and methane; however, these transitions are generally weak in intensity, being induced by magnetic-dipole effects or subtle high-order centrifugal distortion effects. In addition, the rotational Boltzman distributions for temperatures between 300 and 400 K peaks at submillimeter wavelengths for the most important plasma molecules, radicals, and ions.

In the following sections we discuss the application of our submillimeter plasma diagnostic technique on a model reactor for plasma etching, the capacitively coupled gaseous electronics conference (GEC) reference cell.[14] Three applications of the technique are illustrated: (1) the measurement of water-vapor contamination in the reactor and the feed gas by monitoring a rotational transition of H_2O vapor in the reactor just prior to the initiation of the plasma; (2) the assessment of progress in the cleaning of the reactor by an O_2/Ar plasma after a fluorocarbon plasma etch by monitoring the buildup of the concentration of O_3 and the depletion of the concentration of CF_2O in the plasma; and (3) the determination of the endpoint in the etching of a SiO_2 thin film on a silicon wafer by an octafluorocyclobutane/O_2/Ar plasma by monitoring the decrease in the concentration of SiO in the plasma.

II. EXPERIMENT

A. Submillimeter diagnostics tool

Chemical-diagnostic measurements on a model reactor for plasma etching were performed using a submillimeter-wavelength linear-absorption spectrometer, shown schematically in Fig. 1, which is similar to the instrument described by Krupnov and Pavlovsky.[15,16] The submillimeter source is a 450–750 GHz commercial BWO electronic tube. The tube generates approximately 1 mW of output power into a rectangular waveguide. The BWO tube is operated in a magnetic field of approximately 11 kG, produced between the poles of a pair of NdFeB permanent magnets. The frequency of the radiation is tuned by varying the high voltage, typically -3 to -5 kV with respect to ground, applied to the BWO cathode filament. The collector (anode) of the BWO tube is coupled to the laboratory ground through a 100 Ω resistor. A low-level correction voltage is applied to the collector (nongrounded) side of the resistor as part of the phase-locked-loop frequency stabilization circuit.

The radiation from the tube is coupled to a millimeter-wavelength conical horn for free-space propagation. A fraction of the radiation exiting the horn is split off from the main beam by a mica beamsplitter, where it is combined in a harmonic mixer with the output of a frequency-stabilized, 78–118 GHz frequency synthesizer, consisting of a commercially packaged BWO, magnet, high-voltage power supply, frequency-stabilization circuitry, and control electronics. The frequency difference between the BWO and a harmonic of the frequency synthesizer is constrained to 350 MHz by a phase-lock loop, which narrows the linewidth of the BWO to less than 10 kHz. The uncertainty on the absolute frequency is typically limited by the BWO linewidth, as the frequency synthesizer is referenced to a precision low-frequency oscillator, which could be an atomic clock. For the measurements made in this article, sufficient frequency control was obtained using a crystal oscillator.

The submillimeter radiation transmitted through the beamsplitter is collimated by a high-density polyethylene lens (focal length≈15 cm), directed through two quartz windows in and out of the plasma reactor, and then focused by a second identical lens onto a 4.2 K, liquid-He-cooled, InSb,

hot-electron bolometer [NEP$\approx$2 pW Hz$^{-1/2}$, frequency response (-3 dB)$=$750 kHz]. The submillimeter source is frequency modulated at 10–50 kHz for phase-sensitive detection at twice this frequency by dithering the frequency of the 78–118 GHz synthesizer. Typically, a frequency dithering deviation of 0.7 MHz, or about 70% of a linewidth full width at half maximum, is used. Under these conditions, the absorption features appear with a second-derivative line shape. Frequency modulation has the advantage of reducing the base line drift due to standing-wave interference structure prevalent at these long wavelengths. In the case of amplitude modulation, much of the dynamic range of a signal processing system is wasted capturing the base line drift.

Monitoring frequencies for the radicals and molecules of interest are available either directly from the literature or from radioastronomy[17–19] and other databases. It can also be predicted from published spectroscopic constants. The high resolution of the measurements on the order of 1 MHz, limited by Doppler and residual pressure broadening, and the relatively low line density permits the unambiguous identification of an absorption line.

B. Reactive ion etch reactor

All measurements were performed on a capacitively coupled parallel-plate-type reactive ion etcher that was originally based on the standard GEC radio frequency (rf) reference cell.[14] As shown in Fig. 1, several modifications were made to the original GEC configuration. The standard GEC Cell lower electrode was replaced by a custom built electrostatic chuck/powered electrode assembly (model CP100, Electrogrip Inc.) for 100 mm (4 in.) wafer processing. Helium backside cooling pressure was set at 532 Pa (4 Torr) during plasma processing. The electrostatic chuck assembly was cooled by a recirculating coolant at 20 °C inlet temperature. The entire rf powered electrode/electrostatic chuck assembly has a diameter of 150 mm. During the experiments, 200 W of rf power at 13.56 MHz was delivered from a rf generator (RF Plasma Products RF10) through an in-house-built Π-type matching network to the lower electrode to generate plasmas. The center part of the grounded top electrode was a standard GEC electrode (100 mm diameter) with a feed-gas distribution showerhead. The rf conductor of the top electrode was connected to the grounded chamber wall through a copper strap outside of the vacuum chamber. The showerhead/top electrode assembly was also cooled by a recirculating coolant flow at 20 °C inlet temperature. In reactive ion etch, the etch rate depends strongly on the direct current (dc) self-bias and rf voltage at the powered (wafer) electrode. At a given input power, a higher ratio between grounded and powered surface areas leads to an increased dc self-bias voltage[20,21] and consequently increased etch rates. To increase the dc self-bias voltage at the powered (wafer) electrode, the top grounded electrode was extended by a grounded annular ring. With the extension, the grounded electrode has a diameter of 230 mm. The spacing between the grounded and powered electrode is 25 mm. Process gas flows were controlled by a set of mass flow controllers and were fed into the reactor through the showerhead on the top electrode. After passing between the electrodes, the process gases and plasma byproducts were pumped out of the reactor through an 8 in. conflat side port by a 510 l/s turbomolecular pump backed by a multistage dry mechanical pump. The chamber base pressure was about 10^{-5} Pa. During plasma processing, the chamber pressure was measured by a capacitance manometer (MKS Baratron) and controlled by an electronic throttle valve between the reactor and the turbomolecular pump. 5 slm of N_2 was injected into the dry mechanical pump through an interstage pump purge. Part of the plasma effluent exiting from the mechanical pump was sampled by differential pumping and analyzed by a Fourier-transform infrared spectrometer for quantitative analysis of chemically stable reaction products, such as CO, CO_2, and CF_2O. These measurements may, in principle, be correlated with the submillimeter measurements.

III. RESULTS

In the following we illustrate the results of the three applications of the submillimeter chemical diagnostics technique.

A. Measurement of water-vapor contamination

Water-vapor contamination is of concern in many semiconductor manufacturing processes.[22] Submillimeter spectroscopy enables the direct and sensitive measurement of water-vapor contamination in the plasma reactor prior to initiation of the plasma, using the intense $1_{10}-1_{01}$ absorption line at $\nu=556.936$ GHz. The measurement of water contamination is optimally performed without the plasma to minimize water-vapor decomposition and thus enhance detection sensitivity. Alternatively, the OH, H_2O^+, or OH^+ decomposition products could be detected, however, ion concentrations are lower than neutral species by typically two orders of magnitude and the OH radical does not have an intense absorption line within the submillimeter spectral window. We further note that the amount of water-vapor contamination, as judged by the strength of a water vapor submillimeter transition, dropped below our sensitivity level whenever the plasma was initiated, for a range of initial contamination levels of interest.

Monitoring the gas in the reactor allows the quantification of total water-vapor contamination, i.e., that coming from the original feed gas, the transport lines to the reactor, and from outgassing of the reactor walls, which is often the quantity of interest. Performing the measurements just after the chamber cleaning step ensures that the chamber components are at an elevated temperature necessary to produce a water-vapor outgassing level similar to that expected during etching.

In Fig. 2 we show the recorded water-vapor spectra for three 6.65 Pa (50 mTorr) samples in the reactor vessel. The top octafluorocyclopentene (C_5F_8) sample shows no water-vapor contamination at our level of sensitivity of approximately 0.31 μPa (2.3×10^{-6} mTorr) (7.5×10^{7} cm^{-3}) based on a 3σ standard deviation of the signal and the 39 cm pathlength through the reactor. The middle high-purity

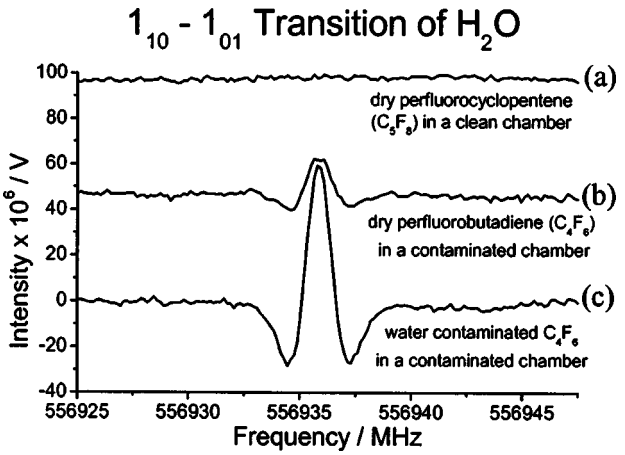

FIG. 2. Spectra of the $1_{10}-1_{01}$ rotational transition of water vapor in the reactor with the plasma off in three different 6.65 Pa (50 mTorr) samples to assess water-vapor contamination from the reactor and the feed-gas stream. The spectra correspond to approximately 30 s of signal averaging. The sample for the top trace (a) was obtained from a flow of 14.3 sccm of octafluorocyclopentene (C_5F_8), 77.1 sccm of Ar, and 18.6 sccm of O_2 and revealed a water-vapor contamination of $<8\times10^7$ cm^{-3}. The samples from the middle (b) and bottom (c) traces were obtained from a flow of 14.3 sccm hexafluoro-1,3-butadiene (C_4F_6), 74.2 sccm of Ar, and 21.5 sccm O_2. The source of the 4.6×10^8 cm^{-3} water-vapor impurity in the middle chamber is a contaminated chamber while the sources of the 1.9×10^9 cm^{-3} water-vapor impurity in the lower trace are both a contaminated C_4F_6 sample and chamber.

hexafluoro-1,3-butadiene (C_4F_6) sample shows a trace level of water-vapor contamination of 4.6×10^8 cm^{-3}, while the bottom lower-purity hexafluoro-1,3-butadiene (C_4F_6) sample trace shows the highest level of water-vapor contamination, 1.9×10^9 cm^{-3}, approximately three times greater than the middle trace based on the ratio of the peak intensities. The spectra were recorded by twice sweeping the submillimeter frequency across the absorption feature using a time constant of 30 ms and a total scan time from 30 to 40 s, and then averaging the two traces. The time response of the system could be reduced by a factor of 3 by minimizing the capture of base line data points outside of the line profile. Further reduction in the time response to <0.5 s could be achieved without significantly reducing sensitivity by capturing just two data points: one at the line center and one outside of the line profile to provide a base line reference.

Application of Beer's law

$$\int \ln[I_0(\nu)/I(\nu)]d\nu = \sigma n \ell_{\text{total}}, \tag{1}$$

allows the determination of the absolute water-vapor concentration in the reactor from the observed integrated line intensities. Here, $I(\nu)$ is the submillimeter radiation intensity at the detector with a gas sample in the chamber, $I_0(\nu)$ is the intensity when the chamber is evacuated or the BWO frequency is off resonance, assuming a flat spectral response of the instrument, $\ell_{\text{total}}=39$ cm is the optical pathlength through the reactor, n is the mean number density of H_2O vapor molecules along the optical pathlength, and $\sigma(T)$ is the integral absorption cross section for the water-vapor line of interest, calculable from available databases.[18] Water vapor absorption of the submillimeter radiation also occurs along the optical path between the source and the reactor, and is partially removed by placing Ar-filled gas cells in the optical path. The remaining laboratory absorption is extremely broad in nature due to pressure broadening, and contributes to the instrument baseline.

At the small, typically parts-per-thousand to part-per-million, fractional absorptions observed in the present study, $\ln(I_0/I)\cong\Delta I/I_0\equiv(I_0-I)/I_0$. Knowledge of both σ and the integrated fractional absorption of the submillimeter radiation by a line allows the direct determination of the integrated column density, $n\ell_{\text{total}}$. If the assumption is made that the absorbing species is distributed uniformly and isothermally within the reactor, which is expected when the plasma is turned off, then n is obtained.

The challenge in the present measurements is in accurately determining $\int\Delta I/I_0 d\nu$ when frequency modulation is used. Here, we have taken the approach of calibrating the observed fractional absorption against the known value for a fixed partial pressure of CF_2O in the reactor, typically 0.013 Pa (0.1 mTorr) (3.1×10^{12} cm^{-3}) produced from 1.3 Pa (10 mTorr) of a gas mixture consisting of 1% by volume of difluorocarbonyl (CF_2O) in N_2. The coincident $44_{4,41}-43_{4,40}$ and $44_{3,41}-43_{3,40}$ CF_2O lines near 558.4 GHz were examined. The cross sections for CF_2O and H_2O were obtained from the database of Pickett *et al.*,[18] assuming a reactor temperature of 300 K. The tabulated cross section for CF_2O was reduced by a factor of $Q_v=1.16$ to account for the nonzero vibrational partition function of the molecule at 300 K; the H_2O cross section has already been corrected for vibrational effects by Pickett *et al.*[18]

The H_2O line intensities were extracted from the measurements by fitting the observed double-derivative line shape profiles to a second-derivative Gaussian line shape function on top of a polynomial base line function to obtain an integrated line intensity. This integrated intensity was referenced against that measured for the CF_2O standard. We note that the theoretical Doppler linewidths are significantly different for these two molecules: 0.41 MHz half width at half maximum (HWHM) for CF_2O and 0.81 MHz HWHM for H_2O. Limiting the accuracy of this calibration method is that the CF_2O reference line is displaced in frequency significantly (≈2 GHz) from the H_2O line, making the calibration prone to errors arising from the change in the spectral response with frequency of the spectrometer.

The absolute sensitivity level obtained for water vapor of 0.31 μPa (2.3 nTorr) (7.5×10^7 cm^{-3}) in the reactor corresponds to a fractional molar concentration of 2.3 nmol/mol (2.3 ppb) for a hypothetical 133 Pa (1 Torr) sample. This level of sensitivity could be improved by signal averaging, multipassing the submillimeter beam through the reactor using a multipass cell or a resonant cavity to increase ℓ, and reducing amplitude noise on the submillimeter radiation. A sensitivity level of 0.5 nmol/mol or 0.5 ppb should be easily achievable, and we eventually expect that levels as small as 0.1 nmol/mol or 0.1 ppb will be possible. At this level of

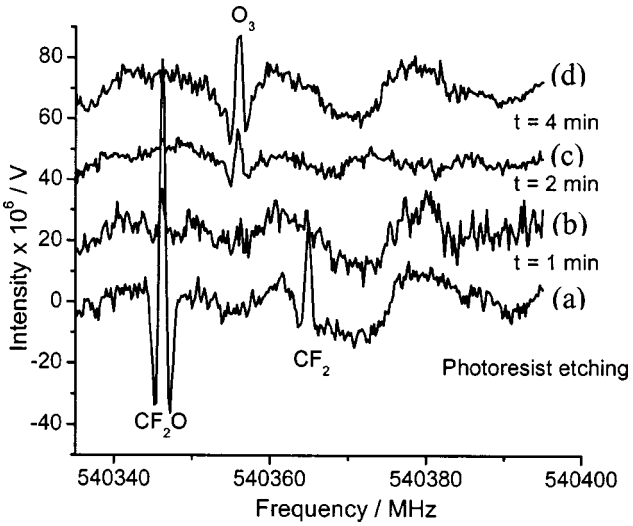

FIG. 3. Spectra as a function of time during the cleaning of a plasma reactor after the etching of a photoresist-coated Si wafer using a plasma formed by flowing Ar, O_2, and C_5F_8 at 77.1, 18.6, and 14.3 sccm, respectively, and at a total pressure of 50 mTorr. The bottom trace (a) was recorded while the photoresist was being etched and shows an unassigned CF_2O line, also observed under plasma-free conditions in a CF_2O:N_2 mixture, and the $18_{2,17}-17_{1,16}$ line of CF_2. The average chamber densities of CF_2O and CF_2 derived from the intensities of these lines are 1.0×10^{13} cm^{-3} and 4.7×10^{11} cm^{-3}, respectively, for the bottom trace. Then the chamber was cleaned with a 50 mTorr Ar/O_2 plasma using Ar and O_2 flow rates of 50 sccm each. The CF_2O and CF_2 transitions rapidly disappear during the chamber cleaning [(b) 1, (c) 2, and (d) 4 min traces], and indeed have effectively vanished after approximately 2 min (2 min trace) into the process. Concomitant with the reduction of these fluorocarbon transitions, the O_3 transition ($11_{5,7}-12_{4,8}$) increases in intensity to a level corresponding to a concentration of O_3 of 1.3×10^{12} cm^{-3} after 4 min, as shown in the top trace (d).

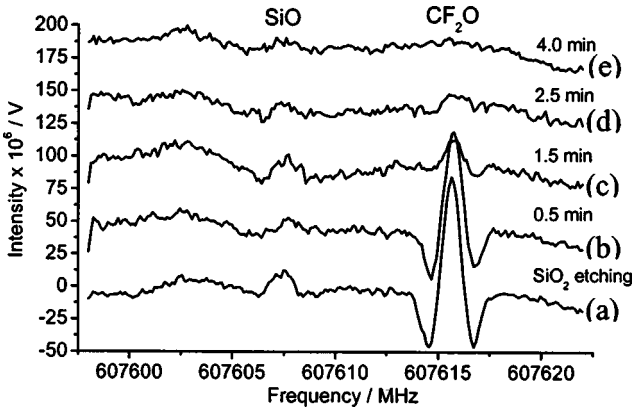

FIG. 4. Spectra observed for an Ar/O_2 cleaning plasma (50 sccm Ar and 50 sccm O_2 at a chamber pressure of 6.65 Pa) following the etching of a SiO_2 layer on a Si wafer by a fluorocarbon plasma (14.3 sccm C_5F_8, 18.6 sccm O_2, and 77.1 sccm Ar at a chamber pressure of 6.65 Pa). The bottom trace (a) shows a spectrum during the etching of the wafer, while the top four traces [(b)–(e)] show spectra recorded from 0.5 to 4.0 min into the cleaning process. The average number density obtained for SiO ($J=14-13$ transition) and CF_2O (unassigned transition) from the bottom trace are 5.7×10^{7} cm^{-3} and 2.0×10^{13} cm^{-3}, respectively.

sensitivity, submillimeter spectroscopy would challenge other water-vapor optical sensors presently in use or under development in simplicity, sensitivity, and cost.

B. Assessment of chamber cleaning progress

To ensure the reproducibility of the multiple plasma processing steps in semiconductor wafer fabrication it is generally desired to clean the reactor chamber at selected intervals during the process. In the present set of investigations, after a wafer was etched it was replaced by a bare silicon wafer and the chamber cleaned by running an equimolar 6.65 Pa (50 mTorr) Ar/O_2 plasma for 4 min, with each gas flowing at 50 sccm. To assess the performance and better understand the complex chemistry of the cleaning process, submillimeter measurements were made of CF_2O, CF_2, SiO, and O_3 transitions in the reactor as a function of time after initiation of the cleaning step. Figures 3 and 4 show some of the results of this study. In both figures, a reference trace is presented at the bottom showing either the etching of a photoresist (Fig. 3) or of SiO_2 on Si (Fig. 4) both using a 6.65 Pa (50 mTorr) mixture of Ar, O_2, and C_5F_8 (perfluorocyclopentene) introduced at a flow rate of 77.1, 18.6, and 14.3 sccm, respectively. In the 540.33–540.40 GHz spectral window of Fig. 3, transitions from CF_2O and CF_2 are observed in the initial trace, while in the 607.595–607.625 GHz spectral window of Fig. 4, transitions from SiO and CF_2O are observed. The transitions from CF_2O are unidentified; the CF_2 transition is assigned as $18_{2,17}-17_{1,16}$ while the SiO transition is assigned as $J=14-13$. The larger scale base line deviations are due to interference from light reflecting off the various optical components in the submillimeter beam path. These interference effects do not result in a significant uncertainty in the absolute measurements since they are very small compared to the magnitude of input light intensity and are subtracted from the measured absorption signals.

Number densities of 1.0×10^{13} cm^{-3} and 4.7×10^{11} cm^{-3} are derived for CF_2O and CF_2 during photoresist etching (bottom trace) in Fig. 3. Number densities of 2.0×10^{13} cm^{-3} and 5.7×10^{7} cm^{-3} are derived for CF_2O and SiO during SiO_2 etching (bottom trace) in Fig. 4. As in the water-vapor contamination study, the absolute fractional absorptions were obtained by referencing the observed integrated intensities to measurements on a known concentration of CF_2O when no plasma was present. The plasma is assumed to have a uniform rotational temperature of $T=300$ K, although experimental studies suggest slightly higher temperatures (300–450 K) with some spatial nonuniformity.[23–27] These absolute number densities are the line averaged result across the entire vacuum chamber and include a relatively long path through the gas surrounding the plasma. Such a situation typically does not occur in most commercial etching reactors.

During the cleaning process, the concentrations of cleaning byproducts (SiO, CF_2O, and CF_2) decrease and effectively vanish below our detection limits as fluorocarbon and silicon dioxide deposits are removed from the chamber wall and internal components. Simultaneous with this decrease, the signal strength of the O_3 rotational line ($11_{5,7}-12_{4,8}$) in Fig. 3 near 540.3 GHz gains in strength, indicating a signifi-

cant buildup of O_3 in the reactor, reaching a peak of 1.3×10^{12} cm^{-3}. The observation that the ozone level increases with chamber cleanliness is consistent with the depletion of carbon-containing deposits which are highly reactive with the O_3. Because the ozone is associated with a cleaned reactor, it should be present regardless of the initial type of wall and surface contamination. The increase of ozone signal strength and the decrease of CF_2O, CF_2, and SiO signal strengths can thus be used to assess the progress of removing residues deposited during the previous plasma etching process.

The high detection sensitivity for SiO of approximately 2×10^7 cm^{-3}, made possible by the large electric dipole moment (1×10^{-29} C m or 3.1 D) and favorable partition function of the molecule, is consistent with the results of Chew *et al.*[13] for the 87 GHz, $J=2-1$ transition of SiO in an electron cyclotron resonance plasma, where they found a sensitivity of 1×10^{11} cm^{-2} for the product of pathlength times number density. Our sensitivity level of 7×10^8 cm^{-2} for pathlength times number density from the $J=14-13$ transition is 150 times smaller than that found by Chew *et al.*[13] for the $J=2-1$ transition. Assuming similar signal-to-noise levels for the two instruments, the factor of 150 greater sensitivity for SiO in the present measurements primarily arises from the 175 times greater line strength for the $J=14-13$ transition relative to the $J=2-1$ transition, and illustrates the advantage of the submillimeter methods over the longer wavelength millimeter methods.

C. Etch endpoint detection

The detection sensitivity of 2×10^7 cm^{-3} demonstrated in the previous section for SiO suggests the possibility of using the concentration of SiO to assess the progress of an etch process. A number of other techniques have been studied for etch endpoint detection, as reviewed by Sun *et al.*,[28] including their tunable diode-laser method. Here, we use SiO measurements to monitor the fluorocarbon plasma etching of a thermally grown SiO_2 layer about 500 nm thick on a Si wafer. In Fig. 5 we show the signal strengths of SiO and CF_2O transitions near 607 GHz at several stages of the etching by an octafluorocyclobutane (c-C_4F_8), O_2, and Ar plasma, at flow rates of 14.3, 7.2, and 88.5 sccm, respectively, and a total chamber pressure of 6.65 Pa (50 mTorr). The top trace (a) of approximately 1 min duration corresponds to two frequency sweeps of the BWO and was acquired at the beginning of the etch process. The initial number densities obtained for SiO and CF_2O under the present conditions are 9.2×10^{14} cm^{-3} and 1.0×10^{14} cm^{-3}, respectively, again assuming a mean reactor gas temperature of 300 K. The second trace (b) of approximately 4 min duration was acquired immediately after the first trace and corresponds to seven sweeps of the BWO. Here, the BWO was continually swept over the spectral window until the SiO signal amplitude was significantly decreased. The third trace (c) was acquired approximately 7 min after the start of the etching process and clearly shows the near total extinction of the SiO signal, whereas the CF_2O concentration is constant. This significant decrease of the SiO signal intensity was a result of complete removal of the SiO_2 layer on the wafer. As seen in the bottom trace (d) in Fig. 5, a residual SiO signal level remains 4 min after the SiO_2 layer had been removed and the underlying crystalline silicon wafer was exposed to the plasma. The low O_2/C_4F_8 ratio in this recipe favored etching of SiO_2 over crystalline silicon. The much lower etch rate of underlying crystalline silicon resulted in the decrease of the SiO signal to a significantly lower residual level once the SiO_2 layer was completely removed. Of course, to obtain a more reasonable time resolution (<0.5 s) in the present study it would be preferable to fix the BWO frequency to the SiO absorption frequency and monitor the signal strength of the SiO transition as a function of time. Such a measurement is straightforward to implement, as the BWO is frequency stabilized and thus easily fixed to a specific frequency.

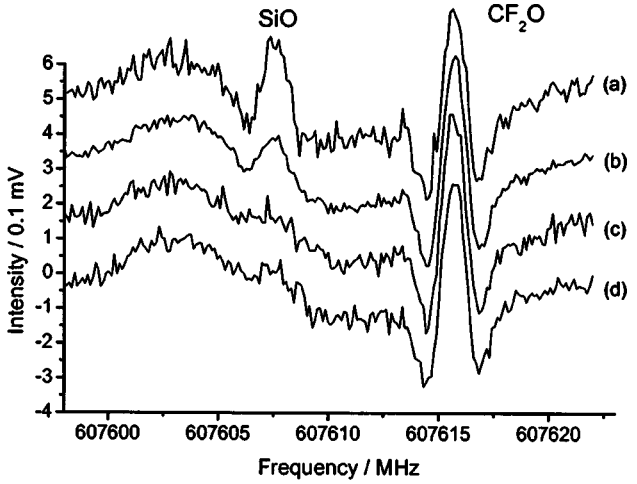

FIG. 5. Spectra observed during the etching of a SiO_2 layer (approximately 500 nm thick) on a Si wafer using a plasma formed by flowing 14.3, 7.2, and 88.5 sccm of octafluorocyclobutane (c-C_4F_8), O_2, and Ar, respectively, at a chamber pressure of 6.65 Pa and showing the $J=14-13$ transition of SiO and an unassigned transition of CF_2O, also present in a pure CF_2O and N_2 mixture. Trace (a) shows the intensities of SiO and CF_2O at the beginning of the etching of SiO_2 and was obtained by sweeping the BWO twice over the two lines over a total time interval of approximately 1 min. The concentrations of SiO and CF_2O at this stage are approximately 9.2×10^{14} cm^{-3} and 1.0×10^{14} cm^{-3}, respectively. Trace (b) corresponds to the average of seven spectral traces over the same frequency interval and was initiated immediately after trace (a) and lasted for a period of approximately 4 min. The trace was acquired to look for evidence of the decrease of SiO. Trace (c) was acquired immediately after trace (b) and was finished approximately 7 min into the etching process and shows that the SiO has nearly vanished due to complete etching of the SiO_2 from the wafer. Trace (d) was acquired 4 min later and shows the SiO concentration remains suppressed from the initial value.

As with many other etch endpoint detection techniques, the present sensitivity is not sufficient to detect endpoints when the ratio of the etched area to the total wafer area is small (i.e., low open area ratio). The present detection sensitivity, however, is useful for detecting the endpoint of removing large areas of silicon-containing films from the inside of a processing chamber. One example of such application is the endpoint detection in cleaning CVD chambers. This technique is particularly valuable for endpoint detection in re-

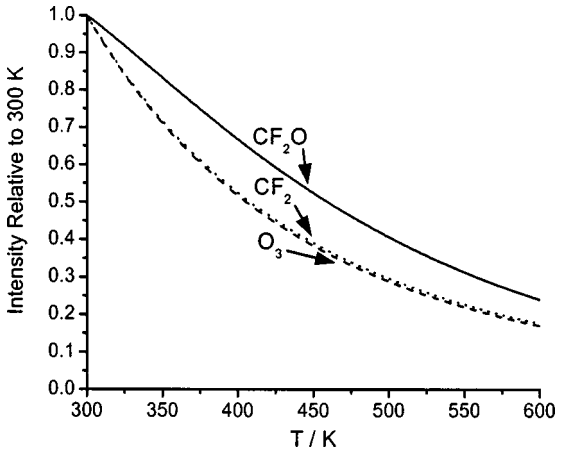

FIG. 6. Intensities of selected rotational transitions of CF_2O ($44_{4,41}-43_{4,40}$ at 558 385.2 MHz), CF_2 ($18_{2,17}-17_{1,16}$ at 540 365.5 MHz), and O_3 ($11_{5,7}-12_{4,8}$ at 540 356.1 MHz) as a function of temperature relative to the 300 K intensities. The translational, rotational, and vibrational temperatures are assumed to be the same.

mote plasma downstream chamber cleaning since traditional optical emission spectroscopy based endpoint detection is no longer viable. Moreover, improvements in sensitivity are possible with multipass schemes based on resonant or nonresonant cavities, potentially allowing the monitoring of endpoints for etch processes with a low open area ratio.

IV. DISCUSSION

The uncertainties in the present density determinations are dependent on the ability to accurately measure the absolute fractional absorption of the submillimeter beam by the plasma. They are also affected by the rotational, vibrational, and translational temperatures of the plasma and their spatial distributions and the chemical nonuniformity of the probed species within the reactor. Here, we will address these uncertainty issues and suggest approaches to quantify and reduce their magnitude.

In Fig. 6 we show for a fixed partial pressure of gas, the relative signal strengths of selected rotational transitions of CF_2O ($44_{4,41}-43_{4,40}$), CF_2 ($18_{2,17}-17_{1,16}$), and O_3 ($11_{5,7}-12_{4,8}$) as a function of the rotational temperature, assumed to be equal to the translational and vibrational temperatures. The translational temperature affects the derived uncertainties through the ideal gas dependence of density on temperature, $n=P/kT$. At a fixed reactor pressure, any increase in translational temperature will result in a concomitant decrease in density. From Fig. 6 we see, for example, that the gas density derived from the signal strength of the CF_2O transition assuming a temperature of 300 K would be nearly 35% too low if the actual reactor temperature was closer to 400 K. For CF_2 and O_3 the effect would be nearly 50%. The similar temperature dependences observed for the CF_2 and O_3 transitions occur because the two molecules have nearly identical vibrational partition functions and the rotational levels probed have similar energies. We note that multipass infrared diode laser measurements give temperatures of the order of 350 K for a capacitively coupled plasma under similar conditions.[25,29]

In principle, relative intensity measurements on different transitions of the same molecule could be used to determine the rotational and vibrational temperatures of the gas, while linewidth measurements could be used to determine the translational temperature of the gas through the $T^{1/2}$ dependence of the Doppler linewidth. Translational temperature determinations from linewidth measurements are difficult due to the relatively narrow transition linewidths of nominally 1 MHz, the need to use frequency modulation to achieve a high level of sensitivity, and the required accuracy necessary to infer the temperature, i.e., a temperature uncertainty of 30 at 300 K requires a linewidth uncertainty of 5% for the Doppler component of a nominally Voigt profile. Such precise Doppler linewidth measurements are further challenged by the presence of residual pressure broadening, typically on the order of 0.075–0.15 MHz/Pa (i.e., 10–20 MHz/Torr) or 0.5–1 MHz absolutely, and power broadening from the many microwatts to milliwatts of submillimeter power.

The present measurements only allow determination of a mean number density and temperature along the optical path. In actuality, both quantities vary along the path, leading to the following expression for the integrated absorbance of a line:

$$\int \ln[I_0(\nu)/I(\nu)]d\nu = \int_0^{\ell_{\text{total}}} \sigma[T(\ell)]n(\ell)d\ell, \qquad (2)$$

where the explicit dependence of the temperature and density on the position along the optical path is shown. Here, T, assumed to be identical to the translational and rotational temperatures taken to be in equilibrium, can be constrained at the reactor wall by the wall temperature. A suitable approximation for $T(\ell)$ and $n(\ell)$ can be used in combination with Eq. (2) to extract density and temperature profiles, as others have reported. Alternatively, the submillimeter path can be varied through the reactor and the data modeled to extract information about the spatial dependencies of the temperature and number densities.

V. CONCLUSIONS

In the present article we described a new and sensitive method for the detection and quantification of chemical species in low pressure [<133 Pa (1 Torr)] plasma reactors. The technique provides the ability to monitor a plethora of molecular species, as nearly all the critical chemical components of semiconductor plasmas have submillimeter wavelength spectra. Although not yet demonstrated to high accuracy, the technique offers the potential to provide quantitative information on the number densities of a variety of chemical species in the reactor, not available by other methods. Future efforts will be directed at developing the submillimeter method into an accurate tool for the quantification and monitoring of chemical species in semiconductor processing plasmas.

ACKNOWLEDGMENTS

The work at the National Institute of Standards and Technology was supported in part by the Advanced Technology Program. The authors wish to thank Air Products and Chemicals, Inc. for permission to publish this work.

[1]N. Hershkowitz, IEEE Trans. Plasma Sci. **26**, 1610 (1998).
[2]N. Hershkowitz and R. A. Breun, Rev. Sci. Instrum. **68**, 880 (1997).
[3]J. P. Booth, Plasma Sources Sci. Technol. **8**, 249 (1999).
[4]D. J. Economou, Thin Solid Films **365**, 348 (2000).
[5]E. Meeks and P. Ho, Thin Solid Films **365**, 334 (2000).
[6]M. Haverlag, A. Kono, D. Passchier, G. M. W. Kroesen, W. J. Goedheer, and F. J. Dehoog, J. Appl. Phys. **70**, 3472 (1991).
[7]C. J. Wang, F. J. Mazzotti, G. P. Miller, and C. B. Winstead, Appl. Spectrosc. **56**, 386 (2002).
[8]K. Takahashi, M. Hori, K. Maruyama, S. Kishimoto, and T. Goto, Jpn. J. Appl. Phys., Part 2 **32**, L694 (1993).
[9]K. Takahashi, M. Hori, and T. Goto, Jpn. J. Appl. Phys., Part 2 **32**, L1088 (1993).
[10]K. Maruyama, K. Ohkouchi, Y. Ohtsu, and T. Goto, Jpn. J. Appl. Phys., Part 1 **33**, 4398 (1994).
[11]M. Haverlag, W. W. Stoffels, E. Stoffels, J. H. W. G. Denboer, G. M. W. Kroesen, and F. J. Dehoog, Plasma Sources Sci. Technol. **4**, 260 (1995).
[12]M. Schaepkens, I. Martini, E. A. Sanjuan, X. Li, G. S. Oehrlein, W. L. Perry, and H. M. Anderson, J. Vac. Sci. Technol. A **19**, 2946 (2001).
[13]K. H. Chew, J. Chen, R. C. Woods, and J. L. Shohet, J. Vac. Sci. Technol. A **13**, 2483 (1995).
[14]P. J. Hargis, Jr. *et al.*, Rev. Sci. Instrum. **65**, 140 (1994).
[15]A. F. Krupnov and O. P. Pavlovsky, Int. J. Infrared Millim. Waves **15**, 1611 (1994).
[16]A. F. Krupnov, Int. J. Infrared Millim. Waves **22**, 1 (2001).
[17]F. J. Lovas, J. Phys. Chem. Ref. Data **21**, 181 (1992); see: http://physics.nist.gov/PhysRefData/micro/html/contents.html.
[18]H. M. Pickett, R. L. Poynter, E. A. Cohen, M. L. Delitsky, J. C. Pearson, and H. S. P. Muller, J. Quant. Spectrosc. Radiat. Transf. **60**, 883 (1998); see: http://spec.jpl.nasa.gov/.
[19]H. S. P. Müller, S. Thorwirth, D. A. Roth, and G. Winnewisser, Astron. Astrophys. **370**, L49–L52 (2001); see: http://www.ph1.uni-koeln.de/vorhersagen/index.html.
[20]H. R. Koenig and L. I. Maissel, IBM J. Res. Dev. **23**, 3 (1979).
[21]C. M. Horwitz, J. Vac. Sci. Technol. A **1**, 60 (1983).
[22]S. A. Tison and J. P. Looney, J. Res. Natl. Inst. Stand. Technol. **100**, 75 (1995).
[23]M. Haverlag, F. J. de Hoog, and G. M. W. Kroesen, J. Vac. Sci. Technol. A **9**, 327 (1991).
[24]M. Haverlag, E. Stoffels, W. W. Stoffels, G. M. W. Kroesen, and F. J. de Hoog, J. Vac. Sci. Technol. A **14**, 380 (1996).
[25]J. P. Booth, G. Cunge, F. Neuilly, and N. Sadeghi, Plasma Sources Sci. Technol. **7**, 423 (1998).
[26]J. P. Booth, G. Hancock, and N. D. Perry, Appl. Phys. Lett. **50**, 318 (1987).
[27]K. L. Steffens (unpublished).
[28]H. C. Sun, V. Patel, B. Singh, C. K. Ng, and E. A. Whittaker, Appl. Phys. Lett. **64**, 2779 (1994).
[29]K. Maruyama, A. Sakai, and T. Goto, J. Phys. D **26**, 199 (1993).